Compositional behavior of Raman-active phonons in $Pb(Zr_{1-x}Ti_x)O_3$ ceramics

E. Buixaderas,[1] I. Gregora,[1] M. Savinov,[1] J. Hlinka,[1] Li Jin (靳立),[2] D. Damjanovic,[2] and B. Malic[3]
[1]*Department of Dielectrics, Institute of Physics, Academy of Sciences of the Czech Republic, 182 21 Prague 8, Czech Republic*
[2]*Ceramics Laboratory, Swiss Federal Institute of Technology – EPFL, Lausanne, Switzerland*
[3]*Electronic Ceramics Department, Jozef Stefan Institute, Ljubljana, Slovenia*
(Received 2 June 2014; revised manuscript received 17 December 2014; published 13 January 2015)

A systematic study of the Raman spectra of $Pb(Zr_{1-x}Ti_x)O_3$ (PZT) ceramics has been performed in a broad temperature interval (10–600 K) and a broad Ti/Zr concentration range around the morphotropic phase boundary ($x = 0.25$–0.70). The number of the spectral components was estimated by a standard fitting procedure with damped harmonic oscillators as well as by counting the number of peaks and shoulders with the help of a purposely designed mathematical analysis based on frequency derivatives of the Raman spectra. This last method proves to be very useful to study Raman spectra of disordered materials. For the case of PZT, the comparison with the Raman modes of $PbTiO_3$ allows us to assign the phonon bands on both sides of the morphotropic phase boundary, and the crossover from the tetragonal to rhombohedral phase spectra is clearly visible. However, there are no indications of a systematic splitting of the E-symmetry modes into monoclinic A'-A'' doublets in the morphotropic samples. Detailed adjusting of the response function to the spectrum requires to assume additional Raman-active modes, but this holds for a much broader concentration range than that of the anticipated monoclinic phase. In particular, the lowest frequency transverse optic mode of E-symmetry (soft mode of the ferroelectric phase transition) is split into two components, a THz frequency anharmonic (central modelike) component and a resonant component (at $\omega \sim 80\,\mathrm{cm}^{-1}$), both related to the same normal coordinate. The additional Raman band appearing in this frequency range ($\omega \sim 65\,\mathrm{cm}^{-1}$) at low temperatures is rather associated with the antiphase tilt vibrations of the oxygen octahedra.

DOI: 10.1103/PhysRevB.91.014104 PACS number(s): 77.55.hj, 63.20.−e, 74.25.nd, 77.80.bg

I. INTRODUCTION

Since the prediction of a monoclinic phase in lead zirconate titanate $Pb(Zr_{1-x}Ti_x)O_3$ (PZT [100 - X]/X, where $X = 100x$), numerous investigations have been focused on probing experimentally its existence. The evidence of this phase is, however, subject to many difficulties due to the intrinsically disordered nature of PZT. The monoclinic phase should act as a bridge between the tetragonal and rhombohedral sides of the phase diagram, near the so-called morphotropic phase boundary ([MPB] near the 50/50 composition). It was related to a shift of the off-centred Pb atom from the tetragonal axis site to the rhombohedral axis one within a monoclinic symmetry mirror plane (the polarization rotation mechanism) [1,2]. Also this phase is now thought to be the cause of the pronounced and well-known dielectric and piezoelectric properties of PZT [3], although its exact role is still only poorly understood. High piezoelectric values of PZT are at least partially associated with the dense domain structures observed near the MPB [4] and with the intrinsic contribution due to the peculiar free energy landscape, which probably enables the phase coexistence [5,6]. Since the experiments do not rule out the presence of the monoclinic phase mixed with other phases [7–9], the symmetry of PZT ceramics at the lowest temperatures near the MPB is still under debate [10,11], even after the very recent structural studies using larger PZT single crystals [12,13].

Among other experimental techniques, Raman spectroscopy was repeatedly employed to study the phonon spectra of PZT ceramics [14–19] in order to verify their phase content and symmetry. In principle, the plausible ferroelectric phases can be distinguished by the number of Raman-active modes. For example, assuming a full B-site occupational disorder and an effective, average Zr/Ti atom, the $PbTiO_3$-like ($Z = 1$) *tetragonal* ferroelectric phase has $3A_1 + 4E + B_1$ Raman-active modes; the ($Z = 1$) *rhombohedral* ferroelectric phase has $3A_1 + 4E$ Raman-active modes plus the silent A_2; and the ($Z = 1$) *monoclinic* ferroelectric phase has $7A' + 5A''$ Raman-active modes. Here the A_1, E, A', and A'' modes are all simultaneously infrared (IR) active and thus subject to the splitting into the transverse optic (TO) and longitudinal optic (LO) components. As far as we know, the monoclinic phase was for the first time supported by a Raman experiment in Ref. [17]. Also, a more recent work [19] assigns monoclinic symmetry to PZT ceramics with $x = 0.48$. However, there is no consideration about cation disorder, angular dispersion, phonon confinement, or doubling of the unit cell at low temperatures [20] in these studies. All these effects either activate new phonon modes in the Raman and/or IR spectra [16,19,21,22] or could lead to the formation of a complex line shape spectral anomalies.

In this paper, we provide a detailed systematic Raman investigation of PZT ceramics, covering a wide range of compositions, temperatures, and Raman frequencies. Spectra are analyzed with the aim to identify spectral changes associated with the change of Ti/Zr composition at different temperatures. This allows revisiting the conclusions on the phase symmetry determination from Raman spectra. It appears that the Raman spectra can be interpreted in agreement with the assignments derived from the analysis of the available far-IR and time-resolved terahertz (THz) spectra [23], and the Raman scattering can be used to estimate the Ti/Zr concentration and to distinguish between the tetragonal and the rhombohedral phases [24]. However, we shall argue that Raman scattering does not give a straightforward evidence for macroscopic monoclinicity in PZT.

II. EXPERIMENTAL

All PZT ceramics were prepared by a conventional solid-state process using standard mixed-oxide route using PbO, TiO_2, and ZrO_2 starting powders of 99.9% chemical purity. PZT ceramics with $x = 0.42$, 0.55, and 0.58 were prepared at the EPFL in Lausanne. The density of the samples was higher than 97% of the theoretical one, and the grain size was about 10 microns. More technical details about the preparation can be found in Ref. [25]. Morphotropic PZT ceramics with $0.45 \leqslant x \leqslant 0.52$ were prepared at the Materials Research Laboratory, Pennsylvania State University. A more detailed description can be found in Ref. [2]. Samples with $x = 0.25$, 0.64, and 0.70 were prepared in the Jozef Stefan Institute in Ljubljana by the solid-state synthesis from constituent oxides PbO (Sigma, 99.9%), TiO_2 (Alfa, 99.8%), and ZrO_2 (TZO, Tosoh), following the procedure described in Ref. [26]. Samples with $x = 0.25$ and 0.64 were prepared by sintering at 1250 °C for 2 h and had a relative density higher than 97%. The sample with $x = 0.70$ was hot-pressed at 1000 °C for 2 h and uniaxial pressure of 24.5 MPa, showing a relative density of 99.5%. Our dielectric and calorimetric measurements of the PZT samples showed a decrease of T_C from 696 to 650 K on decreasing the Ti content from 0.58 to 0.42, in agreement with Jaffe *et al.* [27]. To complement Raman scattering experiments, the samples were characterized by low-frequency dielectric measurements (10^2–10^6 Hz) with a Hewlett-Packard 4192A impedance analyzer. For this purpose, gold electrodes were sputtered onto the faces of the ceramic plates (about 1-mm thick).

Raman spectra were excited with the 514.5-nm line of an Ar laser at a power of 25 mW (∼4 mW on the sample) and recorded in back-scattering configuration using a RM-1000 Renishaw Raman microscope, equipped with a grating filter enabling good stray light rejection, in the 10–900 cm^{-1} range. The diameter of the laser spot on the sample surface amounted to 2–3 μm. A THMS-600 cell (Linkam) was used for temperature control of the samples from 80 to 800 K. For lower-temperature spectra (between 300 and 10 K), some samples were placed in a continuous-flow He cryostat (Oxford Instruments Microstat), and the microscope was equipped with a special angled arm carrying a x20 ULWD objective for efficient optical coupling. The spectral resolution was better than 2 cm^{-1}. The incident laser was linearly polarized, but no analyzer of the Raman scattered light was used. Before the fitting and spectral analysis (see below), spectra were corrected for the instrumental function of the microscope and the Bose-Einstein thermal factor [28].

III. EXPERIMENTAL RESULTS

A. Dielectric measurements

Selected samples were characterized by dielectric measurements before or after the Raman scattering experiment. Samples were typically heated and cooled in the temperature range of 10–720 K at a rate of 1 K/min under a field of ∼5 V/cm. In Fig. 1, we show the permittivity and dielectric loss for selected compositions: tetragonal 42/58; rhombohedral 58/42; and morphotropic samples 50/50, 52/48, and 53/47. The ferroelectric anomalies are seen in the range

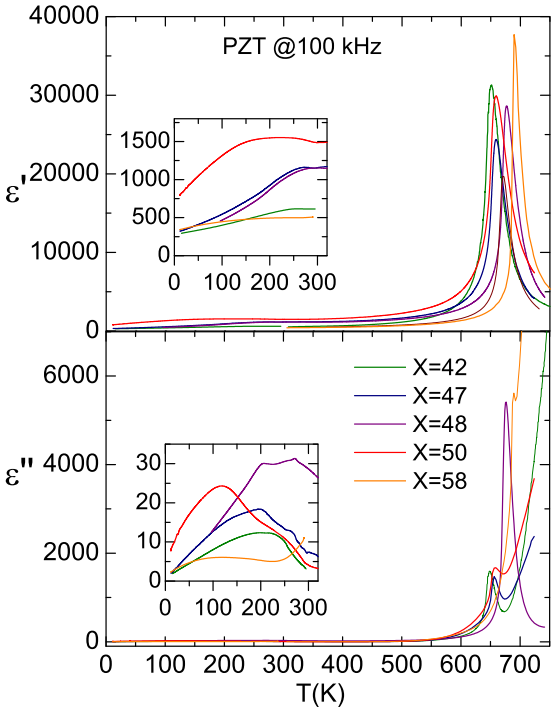

FIG. 1. (Color online) Temperature dependence of the permittivity and dielectric loss of several PZT ceramics at 100 kHz.

600–700 K, in agreement with the known phase diagram and dielectric behavior of these materials [27]. The insets show detailed low-temperature measurements: a clear anomaly is seen in the loss spectra of all the samples below room temperature, accompanied by a change in the slope of the permittivity. This anomaly is related to the gradual appearance of the oxygen octahedra tilt [23,29].

B. Raman spectra

In Fig. 2, the spectra of several PZT ceramics are presented at several temperatures, with Ti content ranging from 25 to 70%. The spectral range can be divided into three regions, according to Ref. [30]. Detailed labeling of the Raman modes was done according to that proposed for, e.g., tetragonal lead lanthanum zirconium titanate (PLZT) [20] and $PbTiO_3$ [31]. In the first region, below about 200 cm^{-1}, modes related to Pb atoms appear (Last type). In tetragonal samples ($x < 0.52$), it is easy to identify the E(TO1) and A_1(TO1) modes at frequencies similar to those modes in $PbTiO_3$ (∼80 and 150 cm^{-1}, respectively). In the second region, between 200 and 450 cm^{-1}, modes from the Zr and Ti atoms show (Slater type). In tetragonal samples, the three main bands correspond to the E(TO2) mode, the $B_1 + E$(TOs) peak stemming from the cubic silent F_{2u} mode, and the A_1(TO2) mode. In the highest frequency region, the band between 500 and 650 cm^{-1} contains the E(TO3) and A_1(TO3) modes, a mixture of vibrations of oxygen and B-site atoms, stemming from the Axe IR active mode in the cubic paraelectric phase. Longitudinal optic modes are also detected in the spectra, the weak E(LO2) and A_1(LO2) modes are located between 420–450 cm^{-1}. Above ∼700 cm^{-1}, we observe the E(LO3) and A_1(LO3) modes with a possible contribution of the nonpolar oxygen breathing mode [32].

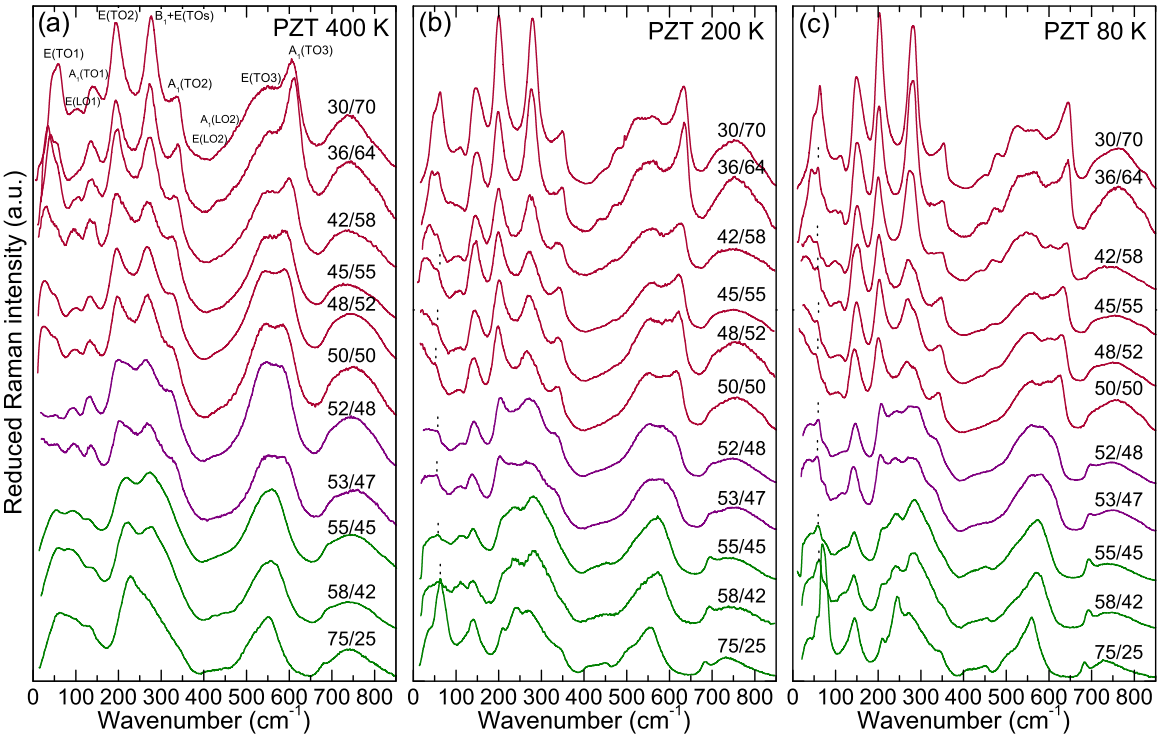

FIG. 2. (Color online) Compositional dependence of the Raman spectra of PZT ceramics at 400 K, 200 K, and 80 K corrected from the Bose-Einstein factor. Labeling of the modes is according to $PbTiO_3$.

Moreover, considerable angular dispersion of polar phonon modes known [33] from single crystal Raman study of $PbTiO_3$ suggests that oblique modes contribute to the Raman band broadening in all PZT compounds.

At 80 K, samples with composition up to 58% Ti are all in the low-temperature phase with a doubled unit cell and additional oxygen-octahedra tilt distortion [21,23]. A doubled unit cell implies an increase in the number of Raman-active modes both in the rhombohedral phase (space group $R3c$) and in tetragonal $I4cm$ phase [23]. A number of additional spectral features is indeed apparent in all spectra of PZT ceramics at 80 K [Fig. 2(c)].

IV. SPECTRAL ANALYSIS

Raman spectra of well-ordered simple single-crystal perovskite materials have normally only a few well-separated phonon lines so that the number of contributing Raman modes corresponds to the number of peaks in the Raman spectrum. However, when the resonant frequencies of two or more such independent lines are located at a distance comparable or smaller than their spectral width, the resulting spectrum could develop a common band with a single maximum. In this case, an asymmetric shape of the band may indicate the presence of the additional mode(s), and, in particular, the additional mode may create a so-called shoulder. Decomposition of such an asymmetric band in distinct contributions is normally done by fitting of the measured line shape to a model with the appropriate number of spectral components. The number of the components in the band has to be specified in advance to perform the fit. If the number of the independent modes in the band is not obvious, it is useful to have a method which allows the identification of the characteristic peaks and shoulders without relying on a particular fitting model. Therefore, we have adopted here also an alternative mathematical procedure for identification of the relevant independent spectral components in the spectrum. This method is based on the location of the curvature maxima in concave-down (CMCD) spectral regions of the recorded Raman spectrum by the analysis of its frequency derivatives. Since the line shapes of PZT Raman bands are visibly very complex and asymmetric, we have systematically analyzed all our data by both methods.

A. CMCD spectral regions

The positions of both "maxima" and "shoulders" can be conveniently cast as locations of the maximum curvature in the downwards bent parts of the spectrum, i.e., as its CMCD points. The CMCD points can be found with the help of the lowest order spectral derivatives of the Raman intensity $I(\omega)$, i.e., $d_1(\omega) = dI(\omega)/d\omega$, $d_2(\omega) = d^2[I(\omega)]/d\omega^2$ and $d_3(\omega) = d^3[I(\omega)]/d\omega^3$. Similar algorithms are also used, for example, in the automatic pattern recognition [34,35]. Let us note that derivatives of the Raman spectra have been also used in the past [36,37] to detect substructure in Raman bands.

Since the curvature is roughly given by the absolute value of the second derivative $|d_2(\omega)|$ and the concave down curvature implies a negative second derivative, $d_2(\omega) < 0$, the CMCD points can be searched as points where the second derivative has a negative minimum. This can be done in two steps: at first, one can locate all positions where $d_3(\omega) = 0$, and second, only those $d_3(\omega) = 0$ positions where the $d_2(\omega)$ has a negative minimum are selected [38].

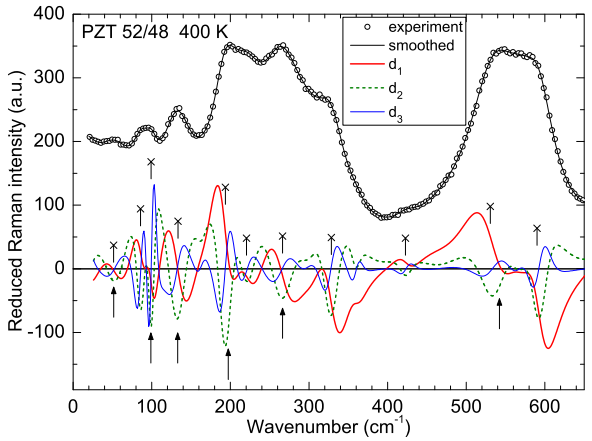

FIG. 3. (Color online) CMCD analysis of the Raman spectrum of the PZT 52/48 ceramics at 400 K together with the simulated smoothed spectrum and its derivatives up to the third order. Arrows denote frequencies of the maxima, and the cross symbols denote CMCD points, defined as negative minima of the second derivative of the spectrum. As explained in the text, CMCD points locate both peak and shoulders of the spectrum.

The practical application of this *CMCD analysis* is illustrated in Fig. 3. In order to avoid noise in the derivatives of the experimental data (open points in Fig. 3), we have first fitted the spectra with an excessive number of components (much higher than the number of anticipated modes), such as Lorentzian and Gaussian functions, to obtain smooth curves but as close as possible to the experimental data. We have checked different options to verify that the results are independent of this step. Then the spectral derivatives of the fitted line (smoothed spectrum) were performed up to the third order (lines in the bottom of the Fig. 3). The negative minima of $d_2(\omega)$ can be found using the conditions $d_2 < 0, d_3 = 0$. They are indicated by cross symbols above the plot of the derivatives. Some of them are in the very vicinity of the maxima of the spectrum ($d_1 = 0$ and $d_2 < 0$, marked by arrows in Fig. 3). Remaining cross symbols indicate the spectral shoulders. With this CMCD method, both spectral features (main peaks and shoulders) can be found in a rather formal way, independently on the more intuitive standard fitting analysis, where the number of modes is imposed explicitly.

B. The standard fit of the Raman spectra

The standard fits of the spectra have been done within a model of independent and damped harmonic oscillators. The number of modes was kept as low as reasonable, having in mind the mode assignment proposed in Sec. III. This constrains the adjusted phonon parameters to have a reasonable physical meaning. Examples of the standard fits are shown in Fig. 4, together with the resulting decomposition. The main differences among the Raman spectra in PZT take place below 400 cm^{-1}.

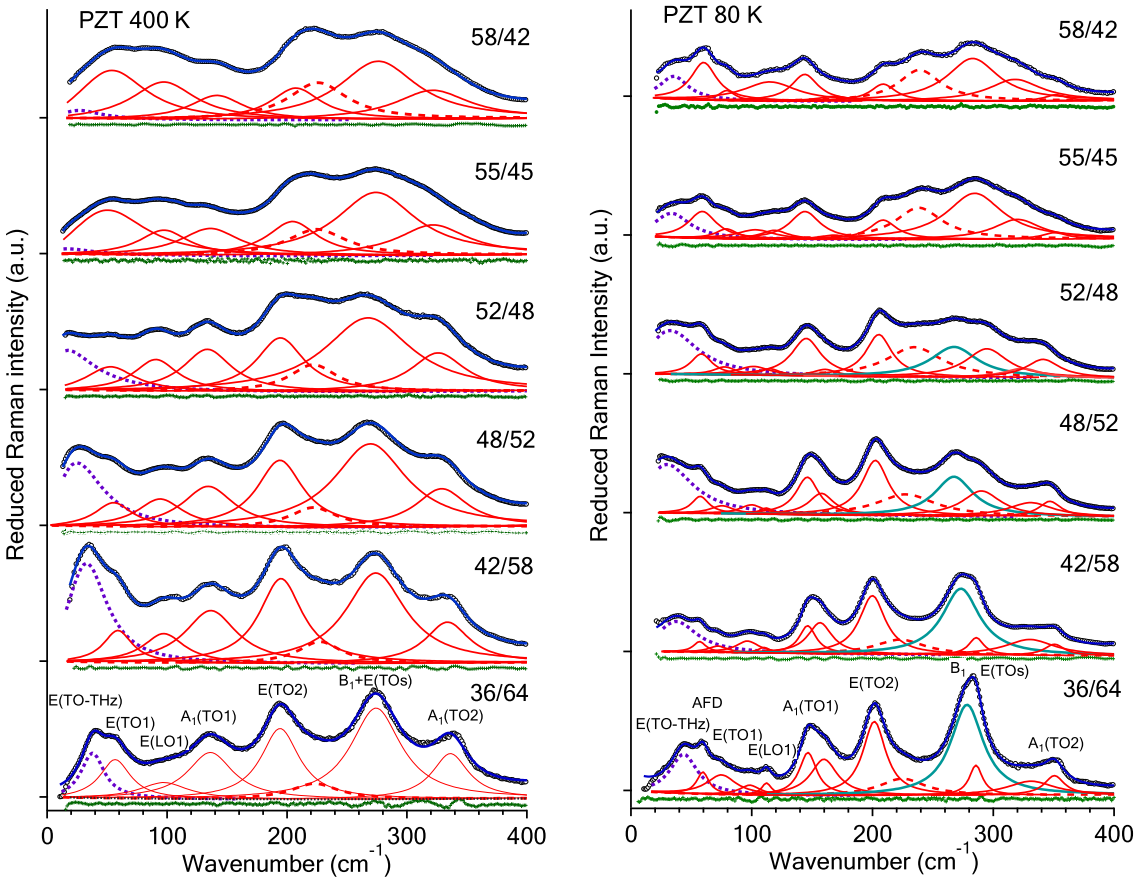

FIG. 4. (Color online) Standard decomposition of the Raman spectra of PZT ceramics at 400 and 80 K by fitting data to the set of independent and damped harmonic oscillator components. Residuals of the fits are also shown below each spectrum. The dotted line shows the E(TO-THz) component of the E(TO1) band; dashed line shows the E(TO2′) component of E(TO2) band.

At 400 K, all samples are in the ferroelectric phase, but above the antiferrodistortive ([AFD] oxygen octahedra tilt) transition. The spectra on the bottom and top of Fig. 4(a) therefore correspond to the rhombohedral $R3m$ and the tetragonal $P4mm$ phase, respectively. There are two interesting aspects in our fits. First, in order to describe the asymmetry of the E(TO2) mode, two damped harmonic oscillator components were systematically included (at $\omega \sim$ 200 and 230 cm^{-1}). The higher frequency component $E(\mathrm{TO2}')$ is shown by a dashed line in Fig. 4. The intensity ratio of these two components turns out to change strongly and reproducibly near the MPB [24]. Second, one needs to add a THz component E(TO-THz) of the E(TO1) mode at low frequencies (dotted line). Both of these features are better seen in tetragonal samples, and they will be discussed in the next section.

At 80 K, several extra peaks are needed to fit the spectra [see Fig. 4(b)]. Since all the samples are in the doubled-cell phase, new phonons activated from the Brillouin zone boundary are expected. In Table I, a list of the Raman phonons measured for three selected compositions at 80 K is presented together with the phonon frequencies found from the far-infrared FIR experiment [23]. The fits are not perfect even taking into account these modes, especially in the tetragonal samples. Nevertheless, the number of peaks in these fits is about the same in all concentration range investigated.

C. Comparison of the standard fit with the CMCD analysis

It is instructive to compare the frequencies of the CMCD points with that of damped harmonic oscillator frequencies obtained from the standard fits. Such comparison is shown in Fig. 5 for 12 different compositions at 400, 200, and 80 K. The CMCD points are denoted by crosses, other symbols linked by continuous lines are damped harmonic oscillator mode frequencies. It can be seen that although both methods rely on a very different strategies, the overall results are quite similar. The assignment of the symmetry types is shown in Fig. 5(a) for the tetragonal side. At 400 K, as expected from group theory, the number of Raman active modes should decrease by one from the $P4mm$ side (right) to the $R3m$ side (left). As the $B_1 + E$(TOs) is effectively merged into one band in the tetragonal side, no change is actually seen at 400 K. This change seems to appear at lower temperatures [Figs. 5(b), 5(c)]. For some compositions towards the rhombohedral side ($x < 0.52$), the AFD mode ($\omega \sim 65\,\mathrm{cm}^{-1}$) is noticeable already at 200 K, and then at 80 K it is seen in all the studied compositions, as well as extra components near all A_1(TO) modes.

Nevertheless, if a macroscopic monoclinic phase were present at the MPB ($x \sim 0.48$), many new phonons would be found near this composition due to the splitting of all E-symmetry modes into $A' + A''$ species. As seen in the plot, this is not the case: there is no indication of a considerable

TABLE I. Frequency and damping constants of the Raman- and IR-active modes in PZT ceramics at 80 K for selected compositions.

		PZT 48/52				PZT 52/48				PZT 55/45			
		Raman		IR		Raman		IR		Raman		IR	
Band	Label	ω	γ	ω	γ	ω	γ	ω	γ	ω	γ	ω	γ
Last	THz	25.1[a]	73.0	31	40.4	30.6[a]	64.5	35.5	49.0	44.4	44.3	41.9	38.0
	AFD	58.2	17.0	65.0	21.0	59.5	19.6	64.5	23.0	60.8	19.9	67.9	13.0
	E(TO1)	76.7	23.7	75.0	50.0	78.4	22.2	76.7	34.0	79.8	25.1	79.2	37.0
	E(LO1)	100.5	23.7	103.0		102.8	32.6			104.9	37.8	108.4	
	$E(\mathrm{LO1}')$	112.3	12.8	114.7		115.6	19.5	122.7		119.6	29.1	124.0	
	A_1(TO1)	146.5	23.0	148.4		145.9	29.7	143.0		144.9	30.5	134.2	
	A_1(LO1)	158.2	25.1	161.2		161.0	23.8			168.5	28.1	138.8	
Slater	E(TO2)	202.8	25.6			205.6	25.9	203.8		209.1	27.5	208.7	
	$E(\mathrm{TO2}')$	225.0	60.0	223.6		236.1	57.4	228.0		239.4	47.1	230.1	
	B_1	268.4	41.7			269.0	48.3						
	E(TOs)	291.4	38.8	292.1		295.7	40.5	292.5		286.1	56.3	280.0	
	A_1(TO2)	331.8	44.7	346.6		324.6	35.9	337.0		321.0	47.5	323.8	
	$A_1(\mathrm{TO2}')$	347.1	22.1	368.8		341.6	33.6	370.0		351.1	25.6	353.9	
	E(LO2)	429.8	26.8	416.3		434.3	41.5	413.9		420.5	17.5		
	A_1(LO2)	465.7	50.2	445.2		474.8	63.2	441.4		447.7	39.1	437.1	
Axe	E(TO3)	527.0	73.8	522.7		527.7	62.3	504.6		521.8	73.8	503.1	
	$E(\mathrm{TO3}')$	562.2	61.6	538.5		559.9	53.6	531.1		556.1	47.0	520.4	
	A_1(TO3)	602.5	39.9	594.0		589.1	37.2	589.8		578.2	34.7	585.2	
	$A_1(\mathrm{TO3}')$	624.6	21.2	632.2		608.5	25.2	617.2		596.8	27.8	628.1	
	$A_1(\mathrm{TO3}'')$	635.8	14.0			622.2	20.4						
	E(LO3)	703.9	26.2			699.4	25.8			693.9	17.2		
	$E(\mathrm{LO3}')$	729.1	42.2			724.4	39.0			721.2	44.3		
	A_1(LO3)	761.4	56.1			756.7	53.8			753.3	59.6		
		801.6	71.7			795.9	76.4			793.3	86.0		

[a]Refers to renormalized frequency ω^2/γ.

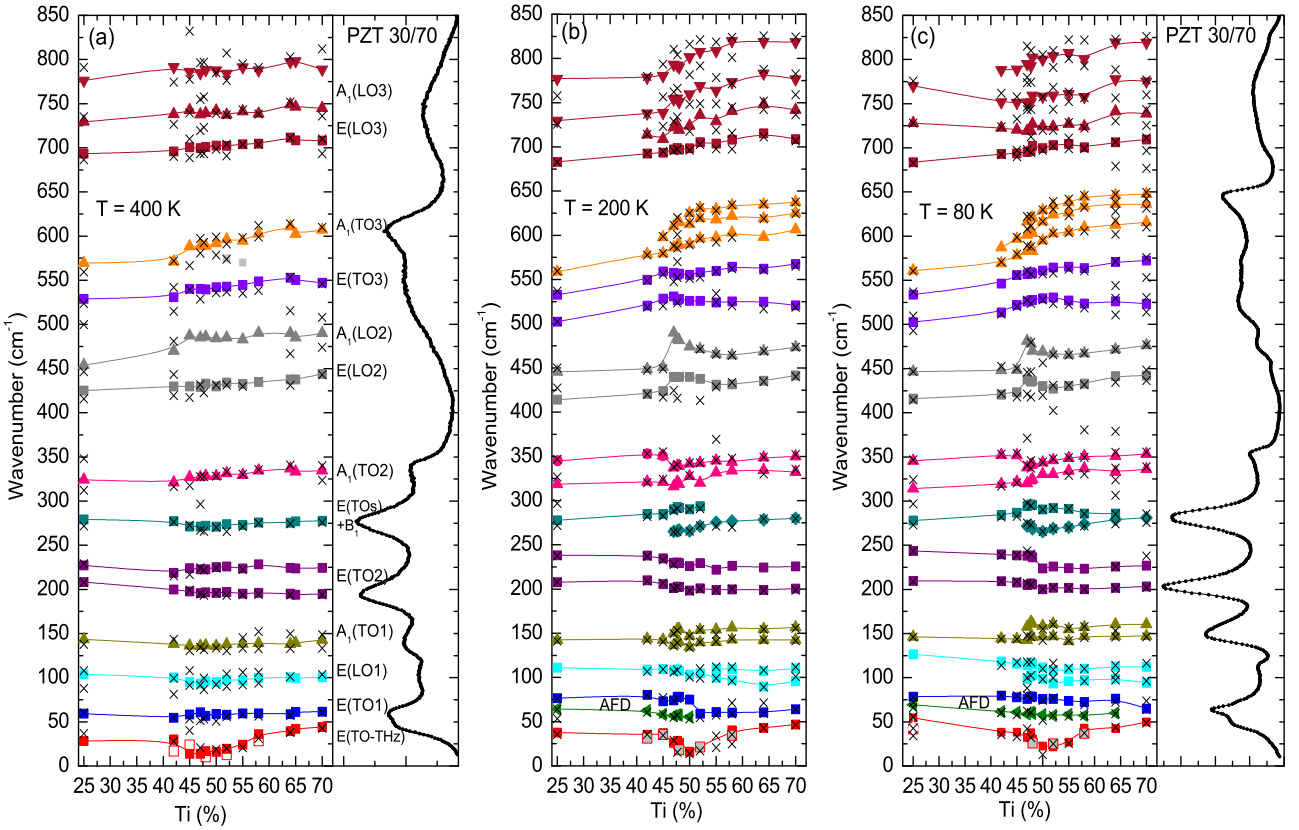

FIG. 5. (Color online) Compositional dependence of the phonon frequencies in PZT ceramics at 400 K (a), 200 K (b), and 80 K (c). Black crosses correspond to the negative minima of the second derivative (peaks and shoulders). Open red squares refer to THz experiment in Ref. [23]. Spectra of the tetragonal sample 30/70 with labels are shown for illustration at 400 and 80 K.

enhancement of the number of distinct mode components in the very vicinity of the MPB.

V. DISCUSSION

Results from the site group analysis presented in Sec. I considered ordered structures with one effective *B* atom in the perovskite lattice. However, in PZT two different atoms are in the *B* position, and, due to their different masses, separate vibrations corresponding to Zr-O_6 and Ti-O_6 octahedra might be seen [39]. In addition, the distribution of Zr/Ti atoms in PZT ceramics is probably not perfectly homogeneous, and Zr/Ti-rich clusters of about 10–20 unit cells size could be present, as found by the Monte Carlo simulations [40]. This, together with the dispersion of oblique modes and the dynamic disorder of Pb atoms, could well explain the richness of PZT Raman spectra [41].

Finally, let us briefly comment on the compositional evolution of other Raman parameters (area and half-width, corresponding to Raman strength and damping constant, respectively), as obtained from the standard fit. Parameters of TO modes from the Last band are presented at selected temperatures in Figs. 6 and 7. The Slater band is shown throughout Figs. 8 and 9.

A. The Last band (Pb related vibrations)

In the high temperature ferroelectric phases [Figs. 6(a), 6(c)], the main phonons within this band are two TO *E*-symmetry modes. The mode in the 60–80 cm^{-1} range was assigned to the *E*(TO1) mode, which corresponds to vibrations of the Pb atom against the octahedra network in the direction

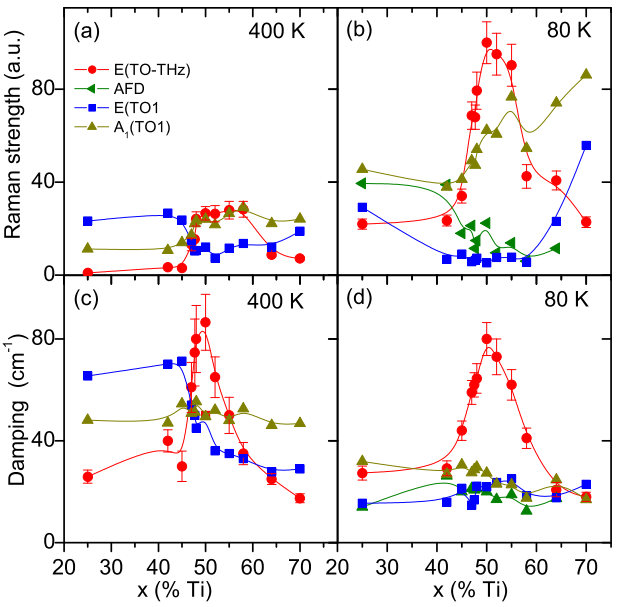

FIG. 6. (Color online) Compositional dependence of the Raman strength and damping constants of the Raman modes in the Last band (below 160 cm^{-1}) for the ferroelectric phase (400 K) and for the tilted ferroelectric phase (80 K).

perpendicular to the spontaneous polarization. This mode is expected to be the main component of the soft mode of the ferroelectric transition; however, in PZT ceramics it softens only slightly. The lowest frequency mode in the THz range, labeled E(TO-THz), seems to have its origin in anharmonic Pb vibrations or hopping among off-center sites, and its frequency softens markedly. At 400 K, these two components exchange their strengths in the MPB region, and the damping constant of the soft THz mode increases steeply towards $x = 0.48$.

At low temperatures [Figs. 6(b), 6(d)], a new peak appears in the 60–70 cm^{-1} range [see, again, Fig. 6(c), corresponding to the AFD mode]. This mode stems from the Brillouin zone corner, and it is activated in the doubled unit cell [42]. The AFD transition (doubling of the unit cell) is accompanied by a small dielectric peak in the permittivity in high Zr-content PZT [43] and by a broad feature in the dielectric loss and the anelastic spectra of the MPB samples [28]. As expected, the Raman strength of the AFD mode, shown by triangles in Fig. 6(b), decreases from the rhombohedral to the tetragonal side. This means that either the tilted phase disappears in samples with $x > 0.64$ or the proportion of the tilted phase diminishes towards the tetragonal side in case of phase coexistence.

Both components of the split soft mode, E(TO-THz) and E(TO1), display similar behavior as at higher temperatures, although the THz component has lower damping and higher strength, and it could be assigned to a new E(TO) mode activated by the unit-cell doubling corresponding to antiphase vibrations of neighboring Pb atoms. Its parameters display a clear anomaly at about $x = 0.50$. As previously found in the IR experiment [23], phonon damping in the MPB region is still anomalously high for low temperatures, which is probably due to the intrinsic disorder of PZT ceramics and the anharmonicity of Pb atoms in the structure. Due to the importance of this mode for the dielectric behavior of PZT, we show in Fig. 7 the dramatic anomalies displayed by its parameters at most of temperatures on crossing the MPB. At high temperatures, the minimum frequency of this mode lies on the $x \sim 0.48$ line; on cooling, however, the minimum is shifted to $x \sim 0.50$–0.52. This agrees with the bending of the MPB towards more tetragonal compositions at low temperatures, as suggested from the FIR data [23]. Damping constants and Raman strengths also show anomalies near the MPB at all temperatures, which indicates that anharmonic lead vibrations play a crucial role in lead-based MPB materials. This mode was already discovered at room temperature in the tetragonal side of the phase diagram [13,14] where it is not overdamped and has a frequency $\omega \sim 50\,cm^{-1}$, although its assignment is not straightforward.

B. The Slater band (Ti/Zr related vibrations)

Parameters of the modes stemming from the Slater band ($\omega \sim 200$–$400\,cm^{-1}$), shown in Fig. 8 for 400 and 80 K, also display anomalies near the MPB. The mode at $\omega \sim 275\,cm^{-1}$ corresponds to the E(TOs) mode on the rhombohedral side and to the doublet $B_1 + E$(TOs) on the tetragonal side. On lowering the temperature, it splits. We assigned the higher frequency component to the E(TOs) mode, as this mode is polar and detected in the IR experiment too, and the lower frequency component to the B_1 symmetry because its strength disappears towards the rhombohedral side [see Fig. 8(b)], where it is forbidden by symmetry. As already mentioned, we have also adjusted the E(TO2) band to two independent components. At high temperatures, these two components exchange their strengths from the rhombohedral to the tetragonal side. Also the damping constants of all the modes show visible anomalies in the MPB region. At low temperature (80 K), the higher frequency component, labeled $E(TO2')$ ($\omega \sim 230\,cm^{-1}$), shows a steep anomaly in its strength crossing the MPB.

The relative ratio of the strength of the first component E(TO2) ($\omega \sim 200\,cm^{-1}$) versus composition can be taken as an indicator of the presence of the tetragonal phase, and it is depicted in Fig. 9 for the high- and low-temperature ferroelectric phases. This ratio is calculated by the simple formula:

$$\text{Relative strength } E\,(\text{TO2}) = \text{Area}_{E(\text{TO2})}/[\text{Area}_{E(\text{TO2})} + \text{Area}_{E(\text{TO2}')}] * 100.$$

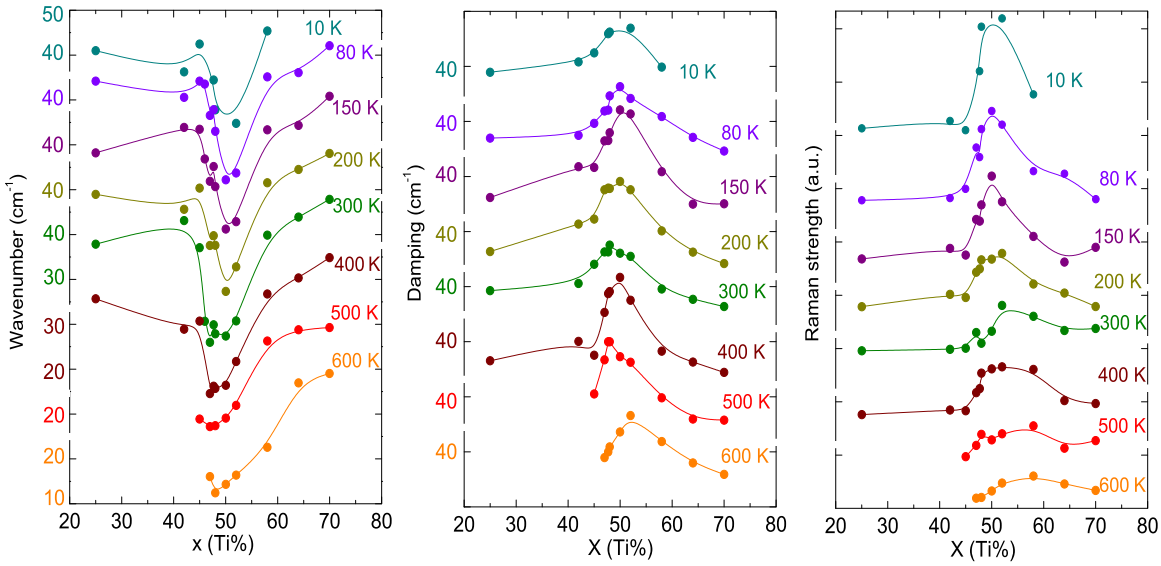

FIG. 7. (Color online) Compositional dependence of the parameters of the soft E(TO-THz) mode in PZT for several temperatures.

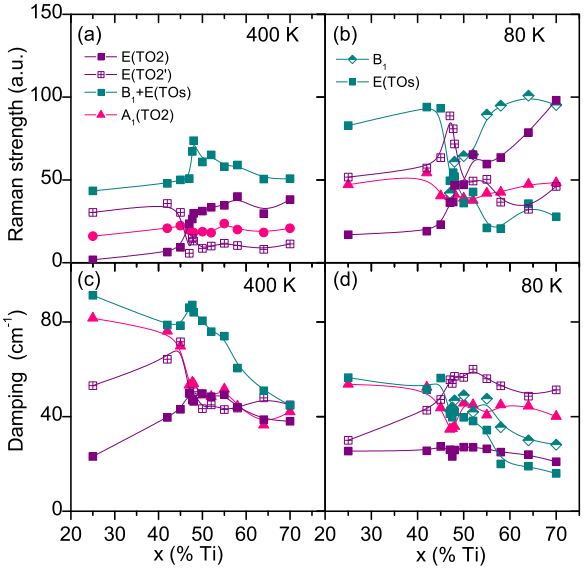

FIG. 8. (Color online) Compositional dependence of the Raman strength and damping constants of the Raman modes in the Slater band for the ferroelectric phase (400 K) and for the tilted ferroelectric phase (80 K).

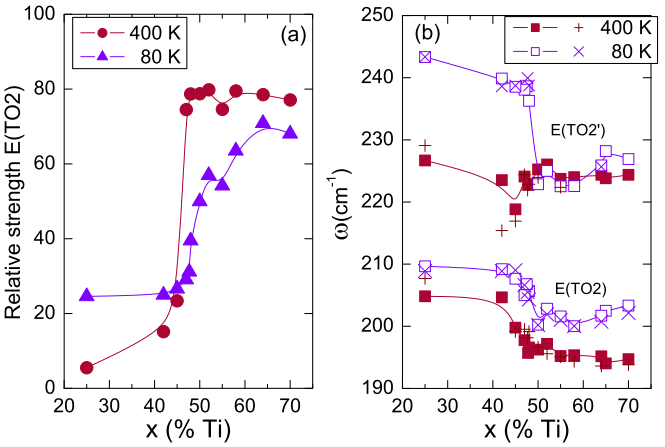

FIG. 9. (Color online) Compositional dependence of the (a) relative strength of the first E(TO2) component ($\omega \sim 198\,\mathrm{cm}^{-1}$) and (b) frequencies of both components in the high-temperature ferroelectric phase (400 K) and in the low-temperature ferroelectric phase (80 K).

The steep change near $x = 0.48$ reveals the presence of the MPB and correlates with the change from the rhombohedral to the tetragonal symmetry, as found in graded PZT ceramics [24]. However, at low temperatures, this change is smoother and extends over a wider range of compositions, which might indicate that macroscopic tetragonal symmetry appears only for $x > 0.50$, whereas in between ($0.45 < x < 0.50$) there can be some phase coexistence or a monocliniclike state. The eigenvector of this mode is related with Ti/Zr atoms, indicating that vibrations of these two atoms in the PZT lattice might also play a role in the development of the MPB.

VI. CONCLUSIONS

A systematic study of the Raman spectra of PZT ceramics in a wide temperature and compositional range has allowed us to analyze fine spectral features reflecting the subtle structural changes in this important dielectric perovskite material. First, the AFD mode was detected for the whole compositional studied range ($x = 0.25$–0.64), confirming the presence of frozen oxygen octahedral tilts in both rhombohedral and tetragonal PZT ceramics at low temperatures at least up to $x \leqslant 0.64$. Second, the measurements confirmed the presence of the strongly damped low-frequency excitation in the THz range, which softens towards the MPB and raises dramatically the Raman signal in this region. Third, the splitting of the $B_1 + E$(TOs) in the tetragonal side and the gradual disappearance of the B_1 Raman-active mode on the rhombohedral side could be observed at low temperatures. Fourth, the abrupt change of shape of the E(TO2) band near the MPB has been documented and quantified.

On the other hand, we did not notice any direct evidence for a monoclinic symmetry, such as splitting of the E-symmetry modes into A'-A'' pairs. The number of the spectral components was estimated by standard fitting procedures as well as by counting of the number of peaks and shoulders with the help of a purposely designed CMCD analysis based on frequency derivatives of the Raman spectra. None of the two approaches could reveal A'-A'' splitting near MPB. Therefore, we have to conclude that the monoclinic structure of PZT ceramics with morphotropic concentrations cannot be directly deduced from the currently available Raman spectra.

ACKNOWLEDGMENTS

The authors thank B. Noheda and R. Guo for providing the morphotropic PZT samples, S. Drnovšek for technical assistance in preparation of some samples far from the MPB, and J. Petzelt for critical reading of the manuscript. This research was supported by the Czech Science Foundation GACR (Project No. 13-15110S).

[1] R. Guo, L. E. Cross, S.-E. Park, B. Noheda, D. E. Cox, and G. Shirane, Phys. Rev. Lett. **84**, 5423 (2000).
[2] B. Noheda, D. E. Cox, G. Shirane, R. Guo, B. Jones, and L. E. Cross, Phys. Rev. B **63**, 014103 (2000).
[3] C. E. Land, P. Thatcher, and G. H. Haertling, in *Advances in Materials and Device Research*, edited by R. Wolfe (Academic Press, New York, 1974), Chap. 4, pp. 137–233.
[4] J. L. Jones and M. Hoffman, Appl. Phys. Lett. **89**, 092901 (2006).
[5] D. Damjanovic, Appl. Phys. Lett. **97**, 062906 (2010).
[6] A. M. Glazer, P. A. Thomas, K. Z. Baba-Kishi, G. K. H. Pang, and C. W. Tai, Phys. Rev. B **70**, 184123 (2004).
[7] M. Hinterstein, J. Rouquette, J. Haines, Ph. Papet, M. Knapp, J. Glaum, and H. Fuess, Phys. Rev. Lett. **107**, 077602 (2011).
[8] D. Pandey, A. K. Singh, and S. Baik, Acta Cryst. A **64**, 192 (2008).

[9] R. Schierholz and H. Fuess, Phys. Rev. B **84**, 064122 (2011).
[10] J. Frantti, Y. Fujioka, J. Zhang, S. Wang, S. C. Vogel, R. M. Nieminen, A. M. Asiri, Y. Zhao, A. Y. Obaid, and I. A. Mkhalid, J. Appl. Phys. **112**, 014104 (2012).
[11] R. S. Solanki, S. K. Mishra, A. Senyshyn, S. Yoon, S. Baik, N. Shin, and D. Pandey, Appl. Phys. Lett. **102**, 052903 (2013).
[12] D. Phelan, X. Long, Y. Xie, Z.-G. Ye, A. M. Glazer, H. Yokota, P. A. Thomas, and P. M. Gehring, Phys. Rev. Lett. **105**, 207601 (2010).
[13] S. Gorfman, D. S. Keeble, A. M. Glazer, X. Long, Y. Xie, Z.-G. Ye, S. Collins, and P. A. Thomas, Phys. Rev. B **84**, 020102 (2011).
[14] G. Burns and B. A. Scott, Phys. Rev. Lett. **25**, 1191 (1970).
[15] J. F. Meng, R. S. Katiyar, G. T. Zou, and X. H. Wang, Phys. Status Solidi a **164**, 851 (1997).
[16] J. Frantti, J. Lappalainen, V. Lantto, S. Nishio, and M. Kakihana, Jpn. J. Appl. Phys. **38**, 5679 (1999).
[17] A. G. Souza Filho, K. C. V. Lima, A. P. Ayala, I. Guedes, P. T. C. Freire, F. E. A. Melo, J. Mendes Filho, E. B. Araujo, and J. A. Eiras, Phys. Rev. B **66**, 132107 (2002).
[18] J. Rouquette, J. Haines, V. Bornand, M. Pintard, Ph. Papet, and J. L. Sauvajol, Phys. Rev. B **73**, 224118 (2006).
[19] M. Deluca, H. Fukumura, N. Tonari, C. Capiani, N. Hasuike, K. Kisoda, C. Galassi, and H. Harima, J. Raman Spectrosc. **42**, 488 (2011).
[20] E. Buixaderas, I. Gregora, S. Kamba, J. Petzelt, and M. Kosec, J. Phys.: Condens. Matter **20**, 345229 (2008).
[21] E. Buixaderas, D. Nuzhnyy, P. Vanek, I. Gregora, J. Petzelt, V. Porokhonskyy, L. Jin, and D. Damjanovic, Phase Transitions **83**, 917 (2010).
[22] E. Buixaderas, V. Bovtun, S. Veljko, M. Savinov, P. Kužel, I. Gregora, and S. Kamba, J. Appl. Phys. **108**, 104101 (2010).
[23] E. Buixaderas, D. Nuzhnyy, J. Petzelt, Li Jin, and D. Damjanovic, Phys. Rev. B **84**, 184302 (2011).
[24] E. Buixaderas, M. Berta, L. Kozielski, and I. Gregora, Phase Transitions **84**, 528 (2011).
[25] M. I. Morozov and D. Damjanovic, J. Appl. Phys. **104**, 034107 (2008).
[26] A. Bencan, B. Malic, S. Drnovsek, J. Tellier, T. Rojac, J. Pavliv, M. Kosec, K. G. Webber, J. Rodel, and D. Damjanovic, J. Am. Ceram. Soc. **95**, 651 (2012).
[27] B. Jaffe, W. R. Cook, and H. Jaffe, *Piezoelectric Ceramics* (Academic Press, New York, 1971), p. 135.
[28] W. Hayes and R. Loudon, *Scattering of Light by Crystals* (Wiley and Sons, New York, 1978), Chap. 7.
[29] F. Cordero, F. Trequattrini, F. Craciun, and C. Galassi, Phys. Rev. B **87**, 094108 (2013).
[30] J. Hlinka, J. Petzelt, S. Kamba, D. Noujni, and T. Ostapchuk, Phase Transitions **79**, 41 (2006).
[31] M. D. Fontana, H. Idrissi, G. E. Kugel, and K. Wojcik, J. Phys.: Condens. Matter **3**, 8695 (1991).
[32] I. Levin, E. Cockayne, M. W. Lufaso, J. C. Woicik, and J. E. Maslar, Chem. Mater. **18**, 854 (2006).
[33] C. M. Foster, Z. Li, M. Grimsditch, S. K. Chan, and D. J. Lam, Phys. Rev. B **48**, 10160 (1993).
[34] R. Neumann and G. Teisseron, Pattern Recog. **35**, 1447 (2002).
[35] O. Niang, E. Delechelle, and J. Lemoine, IEEE Transac. Signal Process. **58**, 5612 (2010).
[36] D. Bauerle, W. B. Holzapfel, A. Pinczuk, and Y. Yacoby, Phys. Status Solidi b **83**, 99 (1977).
[37] J. Frantti and V. Lantto, Phys. Rev. B **56**, 221 (1997).
[38] The maxima and minima of $d_2(\omega)$ may be in principle also distinguished by the sign of the fourth derivative, but in practice, a visual check of the course of $d_2(\omega)$ in the vicinity of each $d_3(\omega) = 0$ position was found to be fully sufficient here.
[39] A. S. Barker, Jr. and A. J. Sievers, Rev. Mod. Phys. **47** (Suppl. 2), S1 (1975).
[40] A. J. Bell, J. Mat. Sci. **41**, 13 (2006).
[41] J. Frantti, Y. Fujioka, A. Puretzky, Y. Xie, Z.-G. Ye, and A. M. Glazer, J. Appl. Phys. **113**, 174104 (2013).
[42] P. Ghosez, E. Cockayne, U. V. Waghmare, and K. M. Rabe, Phys. Rev. B **60**, 836 (1999).
[43] D. Viehland, J.-F. Li, X. Dai, and Z. Xu, J. Phys. Chem. Solids **57**, 1545 (1996).